# Leafhopper-inspired reversibly switchable antireflection coating with sugar apple-like structure arrays

Kuan-Ting Chiang [a,1], Shin-Hua Lin [a,1], Yu-Zhe Ye [a], Bo-Han Zeng [a], Ya-Lien Cheng [a], Rong-Ho Lee [a], Kun-Yi Andrew Lin [b,*], Hongta Yang [a,*]

[a] Department of Chemical Engineering, National Chung Hsing University, 145 Xingda Road, Taichung City 40227, Taiwan
[b] Department of Environmental Engineering, National Chung Hsing University, 145 Xingda Road, Taichung City 40227, Taiwan

GRAPHICAL ABSTRACT
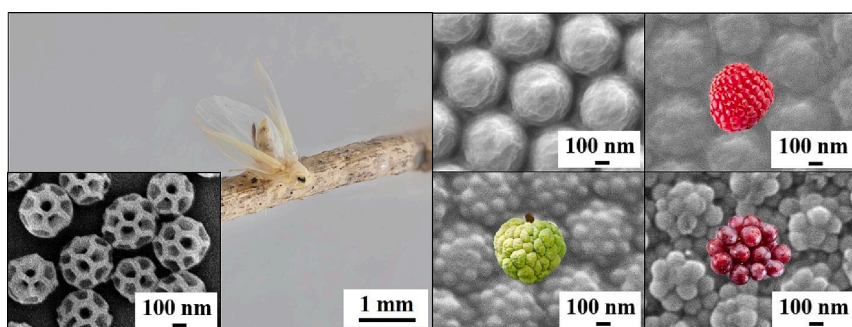
ARTICLE INFO

ABSTRACT

Optical coatings with reversibly tunable antireflective characteristics hold a tremendous potential for next generation optical energy-related applications. Bioinpsired by the camouflage behavior of small yellow leafhoppers, silica hollow sphere/shape memory polymer composites are self-assembled using a non-lithography-based approach. The average visible transmittance of the as-patterned hierarchical structure array-covered substrate is increased by *ca.* 6.3% at normal incident, and even improved by more than 20% for an incident angle of 75°. Interestingly, the broadband omnidirectional antireflection performance can be reversibly erased and recovered by applying external stimuli under ambient conditions. To gain a better understanding, its reversibility, mechanical robustness, and the structure-shape effect on the antireflective properties are systematically investigated in this research.

1. Introduction

Fresnel reflection takes place as incident light propagates through any discrete interface between two media with mismatched refractive indices [1,2]. The light reflection incurs veil glare, energy loss, reduced optical transparency, and vision impairment on diverse instruments and

---

devices. Nowadays, switchable antireflection coatings have attracted tremendous attention over a wide spectrum of applications, including reconfigurable/rewritable optical devices, smart display screens, smart windows, architectural partitions, and next-generation solar energy systems [3,4]. The coatings are able to regulate the amount of light passage in response to external stimuli, and therefore can be reversibly switched between a transparent state and an opaque state on demand. To adjust the light reflection, quarter-wavelength single-layer films and multilayer film stacks are employed to provide destructive interferences [5–7]. In spite of that, the antireflection films are subjected to rare choices of refractive index-matching transparent materials, arduous assembly accuracies, poor stabilities between foreign materials, and narrowband antireflection performances in narrow viewing angles. In view of this, a variety of porous antireflection coatings with appropriately designed refractive indices have been developed through multilayer deposition of particles and oppositely charged polyelectrolytes, stacking of hollow particles, plasma-enhanced chemical vapor deposition, sol–gel processing, phase separation of polymer blends, and many others [8–13]. Unfortunately, there remains a great challenge in establishing a gradual refractive index transition, which is vital for minimizing light reflection in broad operating wavelength regions. Furthermore, the randomly deposited particles considerably scatter incident visible light, and therefore restrict their practical applications.

Over 3.6 billion years of mutations and natural selection, insect species have evolved numerous delicate surface architectures to avoid being tracked by predators in various surroundings. As we know, owl moth (*Brahmaea wallichii*) compound eyes, Cretan cicada (*Cicada cretensis*) wings, longtail glasswing butterfly (*Greta oto*) wings, blue-tailed forest hawk dragonfly (*Orthetrum triangular*) wings, and so forth are covered with sub-microscale protuberances to create graded refractive indices over sufficient heights for eliminating glare as well as light scattering [14–18]. Bioinspired by the adaptive camouflage surface design strategies, miscellaneous sub-microscale structure arrays, such as pyramid-like structure arrays, conical structure arrays, dome-shaped structure arrays, and pillar-shaped structure arrays, have been patterned to emulate the natural antireflective structures [19–24]. Nevertheless, most of the high-aspect-ratio structures are built though exploiting lithography-based fabrication approaches, which require sophisticated equipment along with laborious fabrication processes. Additionally, the artificial structures are restricted to low-resolution features and poor environmental durability. In contrary, colloidal self-assembly approaches offer an inexpensive and straightforward alternative in fabricating high-resolution antireflective structures [25–27]. However, the as-patterned structure arrays, including but not limited to hole arrays, suffer from insufficient structural heights. As a result, the light reflection cannot be effectively suppressed as the angle of incidence varies.

Unlike the aforementioned natural antireflective architectures, hierarchically structured proteinaceous brochosomes are secreted and applied to small yellow leafhopper (*Thaia rubiginosa*) integuments and wings as an anti-wetting and camouflage coating without any extensive coloration [28–30]. The non-sticky brochosomes are sub-microscale granules resembling embroidered balls with pentagonal and hexagonal geometric surface indentations. Early histochemical and enzymological examinations have declared that the brochosomes are mainly composed of proteins (*ca.* 45 ~ 63%) and lipids (*ca.* 19 ~ 30%), bringing about a low surface energy of less than 1.0 mN/m [31–32]. The resulting superhydrophobic properties have been shown to protect leafhoppers from the contamination by their own sticky exudates. Importantly, the presence of three-dimensionally arranged nanoscale air cavities generates refractive index transitions over a wide range of incident angles, leading to omnidirectional antireflective properties and nearly invisible appearances. Once the brochosomal coats are accidentally damaged, brochosomes are rearranged through bouts of vigorously grooming their integuments with legs to recover their antireflective characteristics. Bioinspired by leafhoppers, micrometer-scale metallic synthetic

brochosome particles with ultra-antireflective behaviors have been developed *via* double-layer colloidal crystal template-assisted electrochemical deposition [33,34]. However, the implantation of metals and micrometer-scale structures undoubtedly brings about light scattering and a low optical transparency. Despite recent progress in nanomanufacturing technologies, there remains an enormous challenge to design and build pitted embroidered ball-shaped synthetic mimics. Moreover, the hierarchically porous architectures are limited by low mechanical durability, and hence pose a serious challenge for long-term operating performances.

The recoverable brochosomal coats can even serve as a natural prototype for developing reversibly switchable antireflection coatings. Over the years, diverse stimuli-responsive materials have been invented and exploited to fabricate antireflective structures [35–38]. For instance, the permanent structures of shape memory polymers can be mechanically deformed in rubbery states upon heating through their glass transition temperatures, and the deformed structures turn rigid in glassy states after cooling. Importantly, the temporarily deformable structures can be reconstructed on demands in response to external stimuli, such as heat, ultraviolet radiations, and electric/magnetic fields, allowing them to reverse antireflective characteristics completely. Nevertheless, the physical stimuli-responsive structural transitions suffer from long recovery periods, which considerably impede their applications in integrated devices that desire rapid responses [36]. By contrast, the response speeds of chemical-stimuli-responsive structural recoveries, triggered by applying external chemicals, are much faster [39,40]. Unfortunately, the usage of particular organic solvents inevitably possesses harmful effects on other device components, and incurs adverse health effects. Moreover, current chemical-stimuli-induced shape memory cycles are still restricted to short-term operations.

Benefitting from the booming development of novel materials, ambient-temperature shape memory polymers have been compounded in recent years [41]. Their configurations are switched between permanent and temporary states immediately after drying out of household solvents, such as water and ethanol, under ambient conditions. In this work, the solvent-evaporation-stimulated polymers are introduced to engineer sub-microscale granule arrays with nanoscale silica hollow spheres embedded by a non-photolithography-based fabrication strategy. The leafhopper-inspired broadband omnidirectional antireflective structures are mechanically robust, and can be reversibly transformed on demands, which provide a platform to realize a wealth of intelligent optical applications.

2. Experimental section

2.1. Specimens and reagents

Small yellow leafhopper (*Thaia rubiginosa*) specimens, provided by Taiwan Insect Appreciation Universe Museum, were investigated as received. The chemicals utilized for StÖber silica sphere synthesis and silica hollow sphere synthesis, containing tetraethyl orthosilicate (≥99.0 %), ammonium hydroxide (≥25.0 %), absolute ethanol (≥99.6 %), styrene monomers (≥99.0 %), sodium dodecyl sulfate (≥98.5 %), and potassium persulfate (≥99.9 %), were acquired from Merck KGaA. Deionized water (resistivity 18.2 MΩ·cm at 25 °C) was supplied by a Milli-Q® EQ 7008 ultrapure water system. UV-curable ethoxylated trimethylolpropane triacrylate monomers (ETPTA), UV-curable ethylene glycol diacrylate monomers (EGDA), and 2-hydroxy-2-methyl-1-phenyl-1-propanone (HMPP, Darocur 1173) as a photo-initiator, were purchased from Sartomer Company Corporation, and Ciba Specialty Chemicals, respectively. Hydrofluoric acid aqueous solution (≥48.0 %) was obtained from Merck KGaA. The above chemicals were of reagent quality and were employed without any further treatment. Commercial polyethylene terephthalate (PET) films, provided by Resound Technology Company Incorporated, were rinsed with deionized water before use.
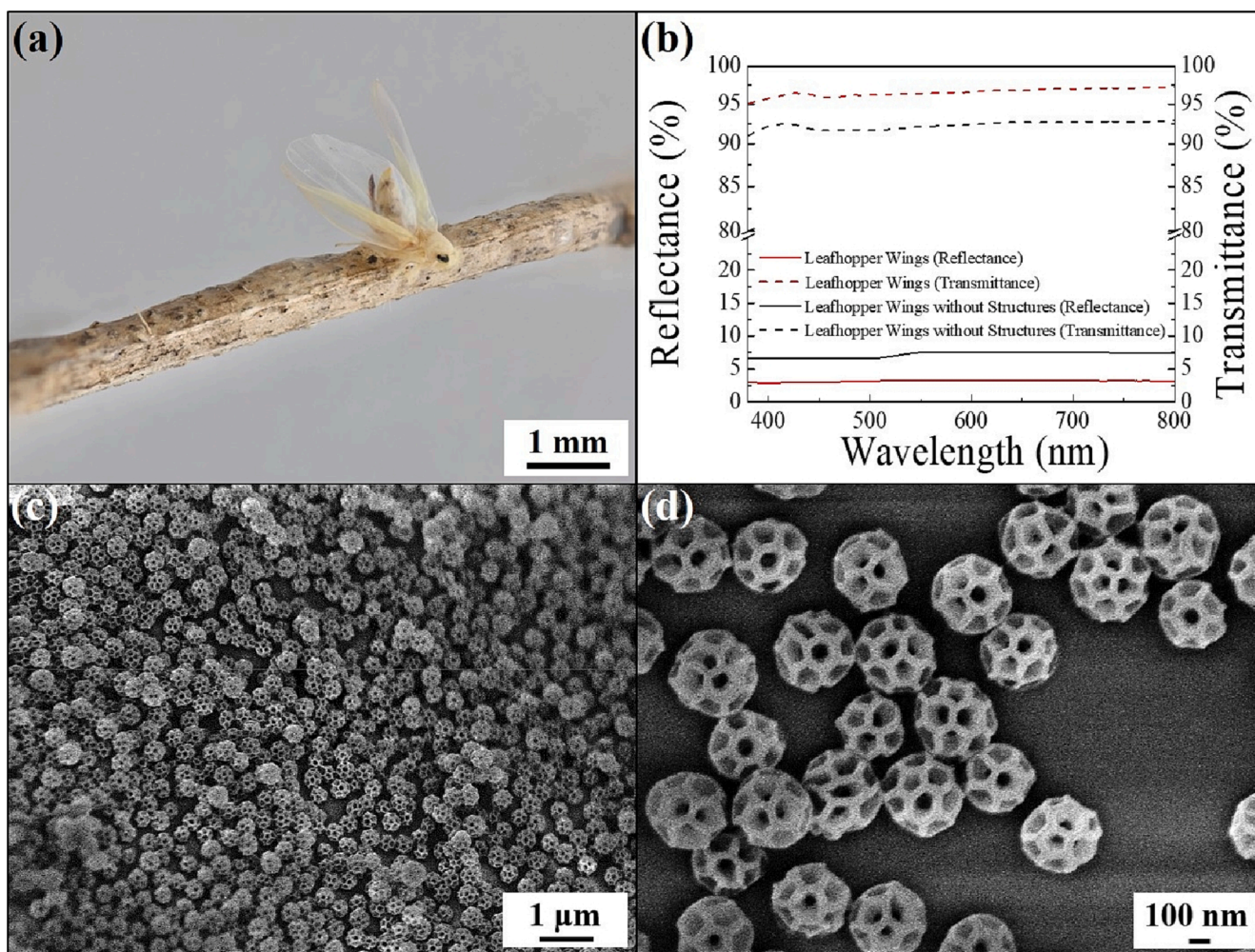
Fig. 1. (a) Photographic image of a small yellow leafhopper taken under natural illumination. (b) Normal-incidence reflectance and transmittance spectra of the leafhopper wings before (red curve) and after (black curve) removing secretory brochosomes. (c) SEM image of the brochosomes. (d) Magnified SEM image of (c). (For interpretation of the references to colour in this figure legend, the reader is referred to the web version of this article.)

2.2. Self-assembly of hexagonally arranged hole arrays

Monodispersed spherical silica colloids, with an average diameter of 450 nm, were synthesized using the well-established StÖber method [42]. After eliminating any unreacted chemical through five centrifugation/dispersion cycles in absolute ethanol, the purified silica colloids were redispersed in a mixture of ETPTA monomer and HMPP (0.5 vol%), and then self-assembled using a modified Langmuir-Blodgett technology. In the assembly process, the as-prepared silica colloidal suspension was continuously dripped on deionized water, in which a rinsed PET film was immersed beforehand. Owing to the large interfacial tension between water and ETPTA monomers, the ETPTA monomer-covered silica colloids rapidly spread onto the water surface, and were spontaneously assembled into a two-dimensionally hexagonal arrangement. Subsequently, the PET film was withdrawn upward with a consistent speed of 2 mm/*sec* using a dip coater (DX-5A, Sadhu Design Corporation), during which the floating monolayer colloidal crystals were transferred onto the film. It is worth noting that the voids between the colloidal crystals and the film were filled by the liquiform monomers during the deposition procedure. After photo-polymerizing the monomers with UV exposure (XLite^TM 500 UV curing chamber, OPAS Corporation), the embedded silica colloids were wet-etched by a diluted hydrofluoric acid aqueous solution (0.5 vol%) to bring about a hexagonally arranged hole array.

2.3. Preparation of silica hollow sphere dispersions

The emulsion polymerization of styrene monomers, stabilized by anionic sodium dodecyl sulfate, was performed in the presence of potassium persulfate as an initiator at 90 °C under nitrogen atmosphere [43]. After rinsing with absolute alcohol to remove residual chemicals, the as-synthesized spherical polystyrene colloids, with an average diameter of 100 nm, were dispersed in a mixture of tetraethyl orthosilicate, ammonium hydroxide, deionized water, and absolute alcohol under vigorously stirring at 45 °C. During the sol–gel process, the hydrolysates of tetraethyl orthosilicate were coupled to construct silica shells onto the polystyrene colloids. The resulting polystyrene-core/silica-shell spheres were then cleansed through another five centrifugation/dispersion cycles in absolute ethanol, followed by calcining at 560 °C until the polystyrene sacrificial templates were completely eradicated. For the hard-template synthesis strategy, silica hollow spheres with adjustable shell thickness and colloid size could be fabricated [44]. Afterwards, the as-prepared silica hollow spheres were dispersed in EGDA monomers consisting of HHPM (1 vol%) by a vortex mixer (Thermolyne 37,600 Maxi-Mix III, Thermo Fisher Scientific Company). The silica hollow sphere volume fraction in the dispersion was controlled to be 95 vol%.
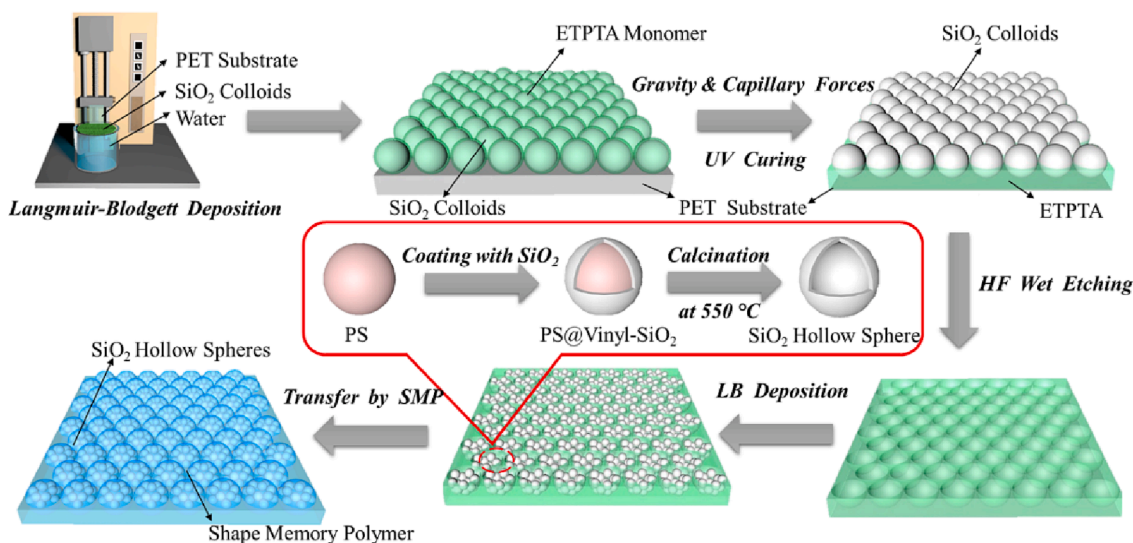
Fig. 2. Schematic diagram of the experimental procedures for engineering sugar apple-like antireflective structure arrays.

2.4. Templating fabrication of hierarchical structure arrays

The EGDA monomer-covered silica hollow spheres were self-assembled, and then transferred onto the hexagonally arranged 450 nm template holes using the aforementioned modified Langmuir-Blodgett technology. After photo-polymerization of the monomers, the silica hollow spheres were temporarily anchored to the holes. Noteworthily, the deposition procedure could be repeated to produce multilayer silica hollow sphere colloidal crystals in demand. Subsequently, the silica hollow sphere-coated template holes were utilized as second-generation templates, on which a mixture of EGDA monomer (84 vol%), ETPTA monomer (15 vol%), and HMPP (1 vol%) was casted and degassed to remove trapped air. The degassing rate was controlled by a micrometering valve set to 5 mL/*sec*. The monomers were finally photo-polymerized to afford shape memory polymer-based hierarchical structure arrays, which could be stripped from the hole arrays effortlessly.

2.5. Instrumentation

Appearances and surface morphologies of small yellow leafhoppers and polymer specimens were characterized with a digital camera (Canon EOS R7, Canon Company Incorporated) and a scanning electron microscopy (SEM) (JEOL 6335F, JEOL Limited Company), respectively. Prior to SEM imaging, the specimens were sputter-coated with uniform gold layers (Cressington 108 Auto sputter-coater, Ted Pella Company Incorporated). Reflectance and transmittance spectra at varied incident angles were conducted by a fiber-optic ultraviolet–visible–near-infrared spectrometer (Optics HR4000, Ocean Optics Company Incorporated) with a halogen-tungsten power source (Optics DT-MINI-2, Ocean Optics Company Incorporated).

3. Results and discussion

Small yellow leafhopper wings are highly transparent under natural illumination (Fig. 1 (a)), allowing the leafhoppers to enhance camouflage against predators. The wings can only reflect less than 3.2% of incident light (red dashed curve), and present a high average transmittance of *ca.* 96.5% in the visible spectral range (red solid curve) (Fig. 1 (b)). This broadband antireflection performance originates from leafhopper-secreted proteinaceous brochosomal coatings (Fig. 1 (c) and (d)). These sub-microscale brochosomes (*ca.* 450 nm in diameter) are with nanoscale pentagonal and hexagonal geometric surface

indentations (*ca.* 100 nm in size) arranged in a three-dimensionally complex periodicity, generating embroidered ball-shaped structural geometries. The intricate hierarchical constructions create a refractive index gradient on the wings and hence suppressing light reflection in the whole visible wavelength region. Importantly, the antireflective characteristics are diminished after scrubbing the non-sticky brochosomes in a bath-type ultrasonicator, operating at 350 W and 20 kHz. The corresponding average reflectance reaches *ca.* 7.2% (black dashed curve), while the average transmittance is decreased by *ca.* 4.0% (black solid curve) (Fig. 1 (b)). The finding discloses that sub-microscale granules with nanoscale air cavities embedded can function as an antireflection coating, though the embroidered ball-shaped hierarchical structures are extremely fragile.

Bioinspired by the leafhoppers, robust artificial brochosome arrays are designed and built through a modified Langmuir-Blodgett technology. Instead of indentations, silica hollow spheres are introduced to generate air cavities. As presented in Fig. 2, ETPTA monomer-covered 450 nm silica colloids, consisting of HMPP as a photo-initiator, are spontaneously assembled into a two-dimensionally hexagonal arrangement on water surface, and then transferred onto a PET film using a dip coater. The self-assembly is induced by the surface tension difference between water and ETPTA monomers. On account of gravitational forces and capillary actions, the monomers can fill the voids between the silica colloids and the PET substrate. After UV-curing, the hexagonally arranged silica colloids are wet-etched to develop a sub-microscale hole array. Subsequently, silica hollow spheres, templated by 100 nm polystyrene colloids, are dispersed in EGDA monomers in the presence of HMPP. The EGDA monomer-covered silica hollow spheres are self-assembled and then deposited onto the as-patterned template holes, during which the monomers also work as an adhesive. Importantly, the above-mentioned Langmuir-Blodgett process can be repeated to deposit demanded multilayer silica hollow sphere colloidal crystals. Afterwards, a mixture of EGDA monomer (84 vol%), ETPTA monomer (15 vol%), and HMPP (1 vol%) is poured gently onto the silica hollow sphere-anchored hole array, and gradually infiltrate into the holes in a degassing process. After exposure to UV radiation, the silica hollow sphere/shape memory polymer composite can be stripped from the template holes to afford hierarchical structure arrays.

To biomimic the structural geometries of small yellow leafhopper-produced brochosomes, sub-microscale hole arrays are fabricated using the Langmuir-Blodgett assembled monolayer 450 nm silica colloidal crystals as templates. Long-range hexagonally arranged poly (ETPTA) hole arrays can therefore be generated after wet-etching the
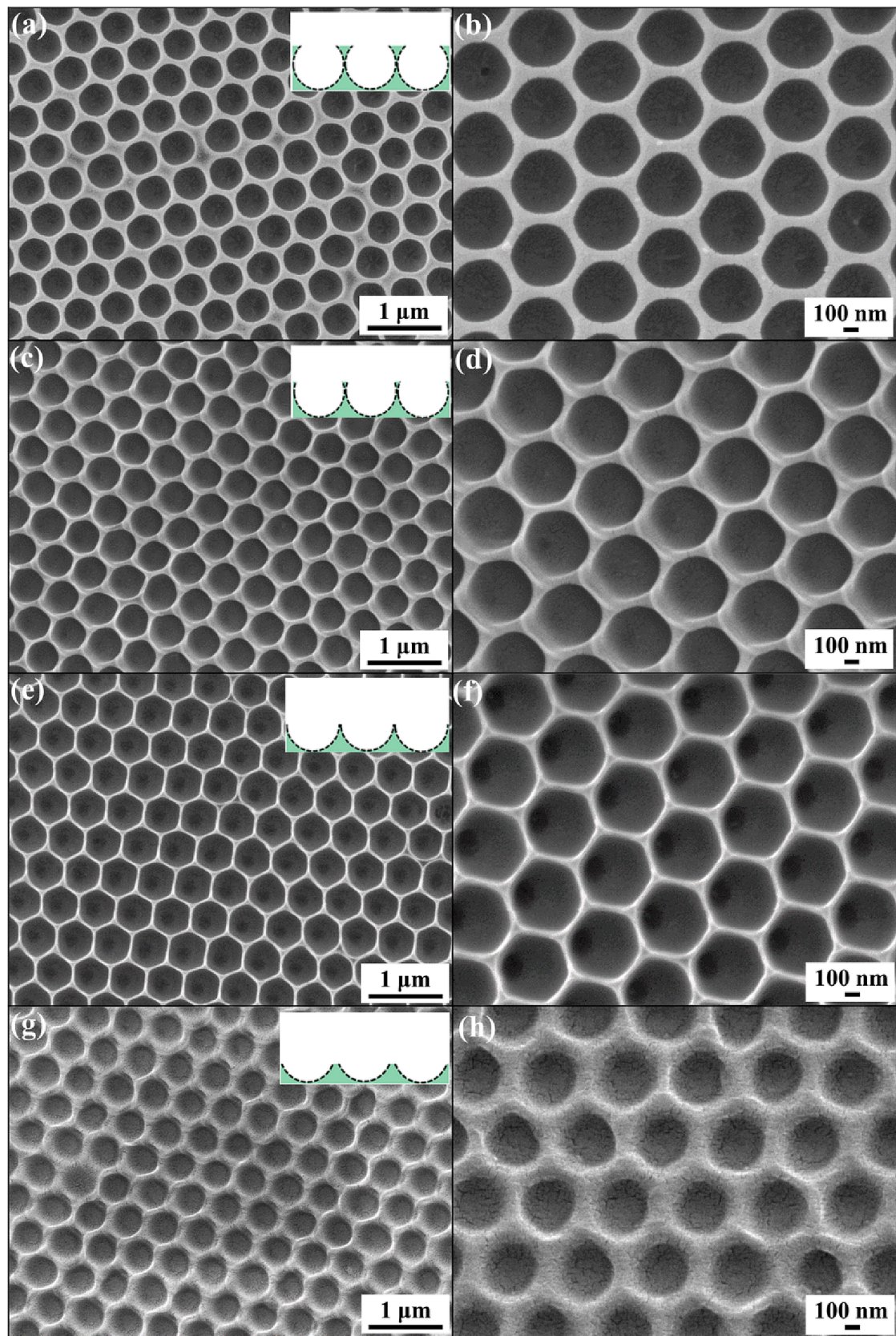
Fig. 3. Top-view SEM images of hexagonally arranged hole arrays templated by monolayer close-packed colloidal crystals using 450 nm silica colloidal suspensions with varied colloid volume fractions. (a), (b) 25 vol%, (c), (d) 30 vol%, (e), (f) 35 vol%, and (g), (h) 40 vol%.
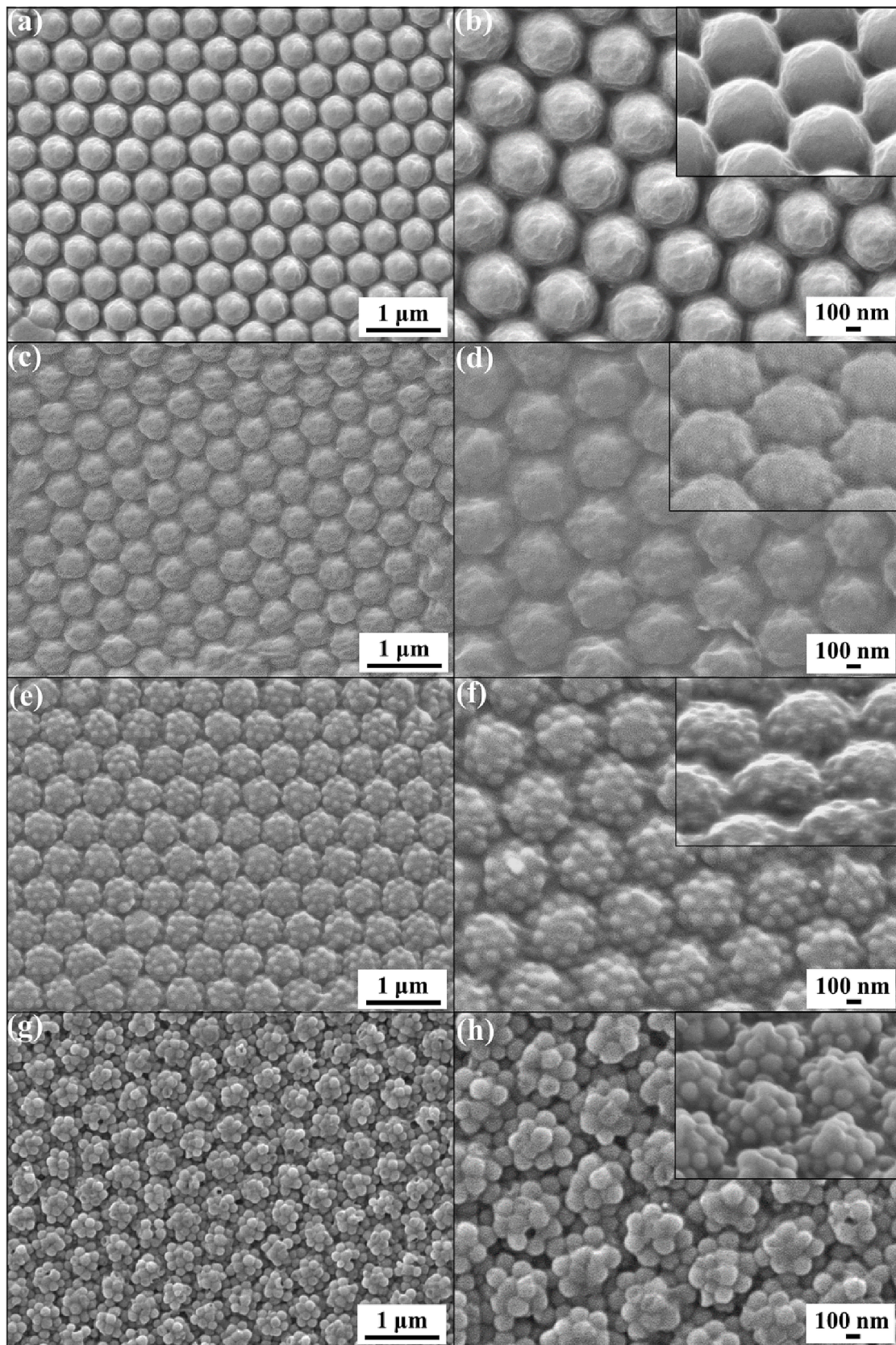
Fig. 4. Top-view SEM images of (a), (b) hexagonally arranged dome arrays, (c), (d) hexagonally arranged raspberry-like structure arrays, (e), (f) hexagonally arranged sugar apple-like structure arrays, and (g), (h) hexagonally arranged grape-like structure arrays. The inserts showing the magnified side-view SEM images.
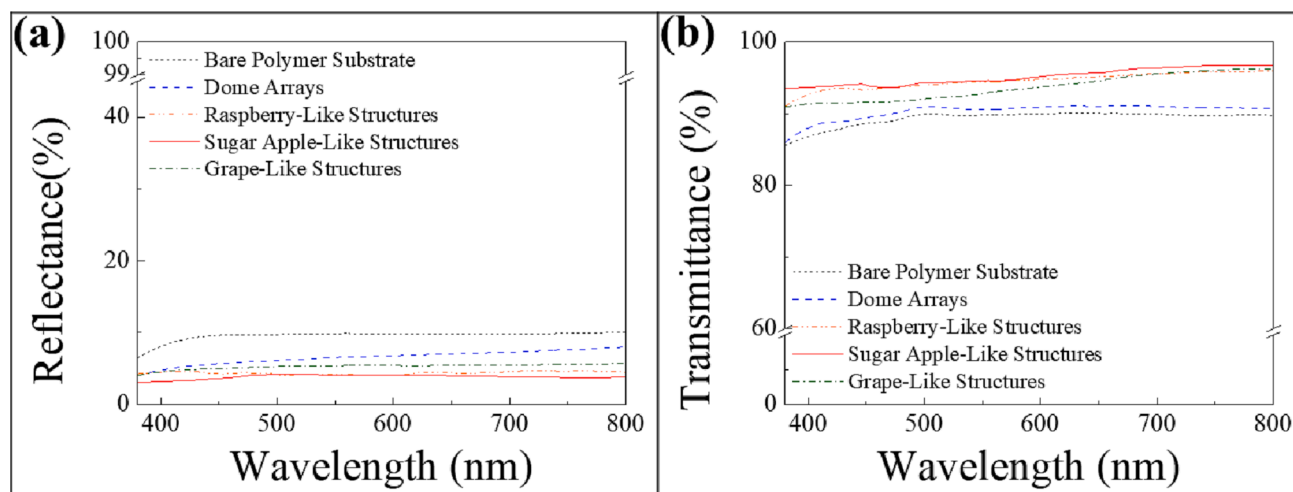
Fig. 5. (a) Normal-incidence reflectance spectra and (b) normal-incidence transmittance spectra acquired from a bare polymer substrate (black curve) and polymer substrates covered with hexagonally arranged dome arrays (blue curve), hexagonally arranged raspberry-like structure arrays (orange curve), hexagonally arranged sugar apple-like structure arrays (red curve), and hexagonally arranged grape-like structure arrays (green curve). (For interpretation of the references to colour in this figure legend, the reader is referred to the web version of this article.)

embedded silica colloids (Fig. 3). Importantly, the introduction of silica colloidal suspensions with higher colloid volume fractions in the self-assembly process leads to the formation of less poly(ETPTA)-embedded silica colloids, and hence brings about template holes with varied opening sizes and depths. It is evident that a hemispherical hole array is created as the colloid volume fraction reaches 35 vol%. Subsequently, 120 nm silica hollow spheres (Fig. S1), templated from 100 nm polystyrene cores, are Langmuir-Blodgett assembled and then deposited onto the hemispherical hole array (Fig. S2). After repeating this deposition procedure, the holes are rinsed with absolute ethanol to remove untrapped silica hollow spheres. Theoretically, each of the holes can be filled with around 16 silica hollow spheres (Fig. S3). The silica hollow sphere-anchored hole array is finally utilized as a second-generation template, on which an EGDA monomer/ETPTA monomer/HMPP mixture is applied as a casting material. It is worthy to mention that the monomer mixture can gradually replace the trapped air and infiltrate into the template holes during a degassing process. As a result, the holes are partially filled with different amounts of monomer mixture as the degassing period varies. After photo-polymerization, silica hollow sphere-embedded hemispherical structure-patterned shape memory polymer substrates can be peeled off from the templates. Clearly, their long-range hexagonal arrangements are well-preserved through the templating fabrication process, though a few blemishes are noticed (Fig. 4). In comparison with the dome array shaped by bare template holes (Fig. 4 (a) and (b)), diverse hierarchical structure arrays are developed using the silica hollow sphere-anchored template holes (Fig. 4 (c)–(h)). The application of shorter degassing period results in less shape memory polymer-embedded silica hollow spheres. Consequently, hexagonally arranged raspberry-like structure arrays (Fig. 4 (c)–(d)), sugar apple-like structure arrays (Fig. 4 (e)–(f)), and grape-like structure arrays (Fig. 4 (g)–(h)) are engineered through varying the degassing periods from 60, 40 to 20 s. All the artificial brochosomes are with *ca.* 450 nm in size and multiple immobilized air cavities (*ca.* 100 nm in size). Importantly, their surface morphologies can also be adjusted through applying varied-sized silica hollow spheres in the Langmuir-Blodgett assembly procedure.

Normal-incidence reflectance spectra and transmittance spectra of the hexagonally arranged hierarchical structure array-covered shape memory polymer substrates are collected and compared in Fig. 5 to evaluate their antireflective characteristics. On account of an abrupt transition in refractive index at the air/polymer interface, *ca.* 9.6% of incident visible light is reflected from a featureless polymer substrate
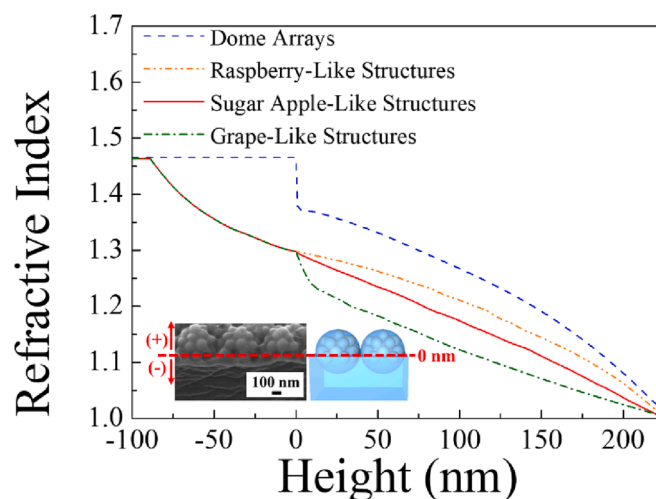

Fig. 6. Computed effective refractive index profiles of the templated structure arrays.

(black dotted curve), thereupon the specimen presents a relatively low average transmittance of *ca.* 89.4% across the entire visible spectrum (380 to 800 nm). It is worthy to note that ca. 1.0% of incident light is absorbed by the specimen. The light reflection can be suppressed by more than 3.0% through patterning a sub-microscale dome array to render a moderate refractive index transition (blue dashed curve). Unanticipatedly, its average transmittance is only increased by *ca.* 1.0%, which is attributed to the internal light reflection and light refraction within sub-microscale structures. In comparison, the antireflection performance can be further reformed by introducing silica hollow sphere-embedded dome arrays to diminish the unfavorable optical impairments. It is evident that the reflectances of as-engineered grape-like structure array-covered specimen (green dash-dotted curve), raspberry-like structure array-covered specimen (orange dash-dotted curve), and sugar apple-like structure array-covered specimen (red solid curve) reach *ca.* 5.3%, *ca.* 4.4%, and *ca.* 3.3%, respectively. Their corresponding transmittances in the visible spectra range are improved expectably, where average transmittances of *ca.* 93.6%, *ca.* 94.5%, and *ca.* 95.7% are achieved. The difference in broadband antireflective characteristics between the hierarchical structure arrays can be
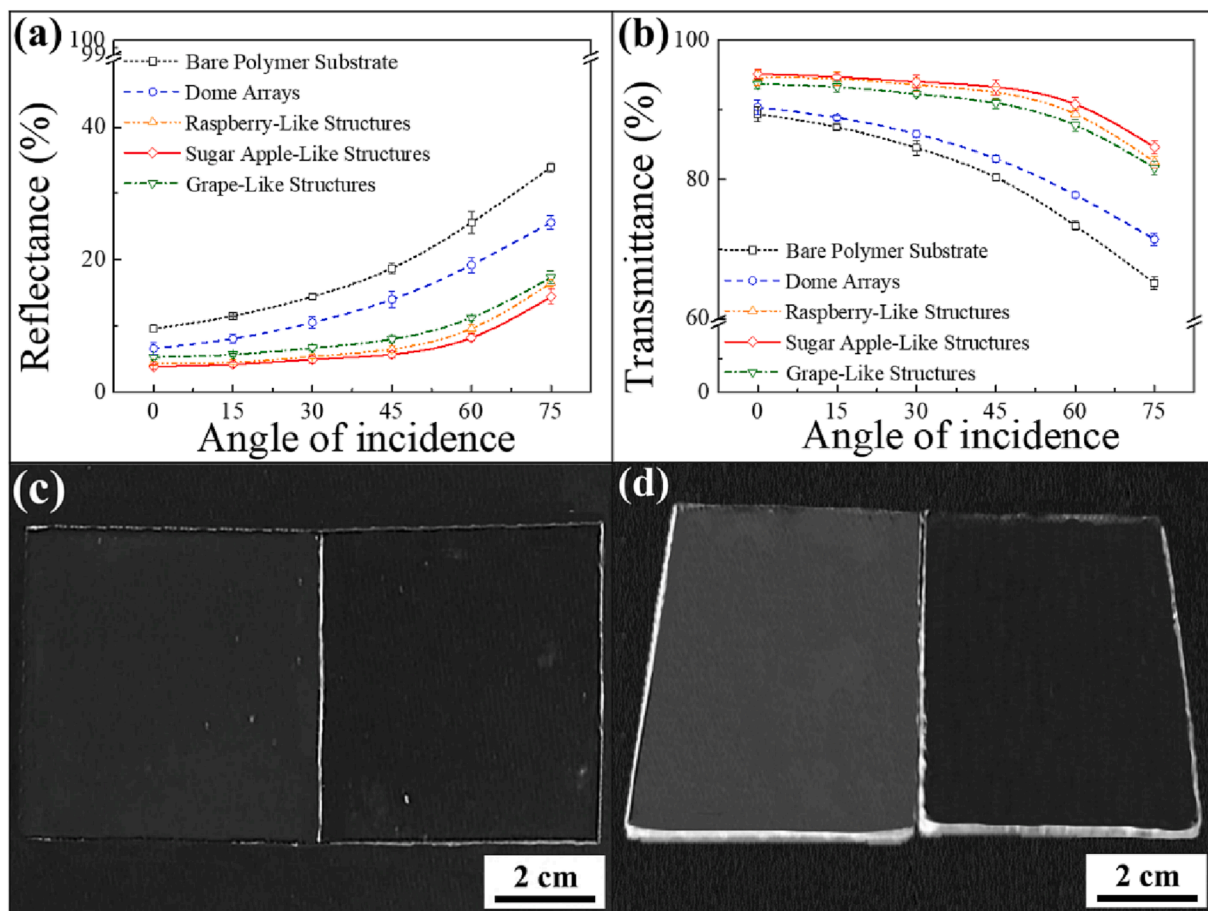
Fig. 7. (a) Average reflectances and (b) average transmittances in the visible spectral range collected from a bare polymer substrate (black curve) and polymer substrates covered with hexagonally arranged dome arrays (blue curve), hexagonally arranged raspberry-like structure arrays (orange curve), hexagonally arranged sugar apple-like structure arrays (red curve), and hexagonally arranged grape-like structure arrays (green curve) at varied incident angles. Photographic images of a bare polymer substrate (the left one) and a polymer substrate covered with sugar apple-like structure arrays (the right one) taken under natural illumination at varied viewing angles of (c) 0° and (d) 75°. (For interpretation of the references to colour in this figure legend, the reader is referred to the web version of this article.)

interpreted from effective refractive index transitions across the templated structures, which are computed using an effective medium theory [45]. As presented in Fig. 6, the sugar apple-like structures possess a smoother refractive index transition and a relatively lower average refractive index at the air/polymer interface (red solid curve), and hence the light reflectance is suppressed more efficiently. Importantly, its antireflection performance (red solid curve) is even superior to polymer substrates covered with hexagonally arranged 450 nm silica colloidal crystals (green dash-dotted curve), 450 nm silica hollow sphere colloidal crystals (orange dash-dotted curve), 120 nm silica colloidal crystals (black dotted curve), and 120 nm silica hollow sphere colloidal crystals (blue dashed curve) (Fig. S4). The findings disclose that either sub-microscale dome structures or nanoscale air cavities are critical to develop antireflective structures.

Toward a better understanding of the artificial brochosomes, optical reflectance and transmittance spectra of the aforementioned hierarchical structure array-covered shape memory polymer substrates are conducted at different incident angles of 15°, 30°, 45°, 60°, and 75° (Fig. S5). Clearly, their average reflectances and average transmittances in the visible spectra range exhibit similar tendencies as the incident angle varies from 0° to 75°. As summarized in Fig. 7 (a) and (b), all the average reflectances increase with the angle of incidence, whereas their average transmittances decrease with the incident angle. It is noticeable that antireflection behaviors of the hierarchical structure array-covered specimens are less sensitive to incident angles. Compared with the optical properties of a featureless specimen (black dotted curve), the

visible light reflection can be considerably reduced by *ca.* 20.5% on a sugar apple-like structure array-covered specimen for an incident angle of 75° (red solid curve), while its average transmittance can surprisingly achieve *ca.* 85.6%. The virtually unchanged antireflective capability over a wide range of incident angles is even competitive with that of small yellow leafhopper wings (Fig. S6). It is believed that the hierarchical structures establish smooth effective refractive index transitions at varied incident angles, thus bringing about a broadband omnidirectional antireflection performance. The photographic images of a bare specimen (the left one) and a sugar apple-like structure array-covered specimen (the right one) taken at 0° (Fig. 7 (c)) and 75° (Fig. 7 (d)) once again demonstrate its omnidirectional antireflective capability. In contrast to appearances of the bare specimen under natural illumination, the hierarchical structure-covered one is highly transparent even at a large viewing angle.

The poly(ETPTA)/poly(EGDA) copolymer-based hierarchical structures can be temporarily deformed or recovered by applying external stimuli at ambient temperature, originated from its low glass transition temperature of *ca* −42 °C [46,47]. Benefiting from the unique shape memory characteristics, the sugar apple-like structure array-covered specimen is rinsed with deionized water, and then dried in air under ambient conditions. The water evaporation-induced capillary force surmounts intermolecular interactions between the water-swollen copolymer chains; hence, the templated sugar apple-like structures are distorted and squashed (Fig. 8 (a)) [48,49]. Owing to the increased van der Waals attraction forces within the compressed copolymer chains, the
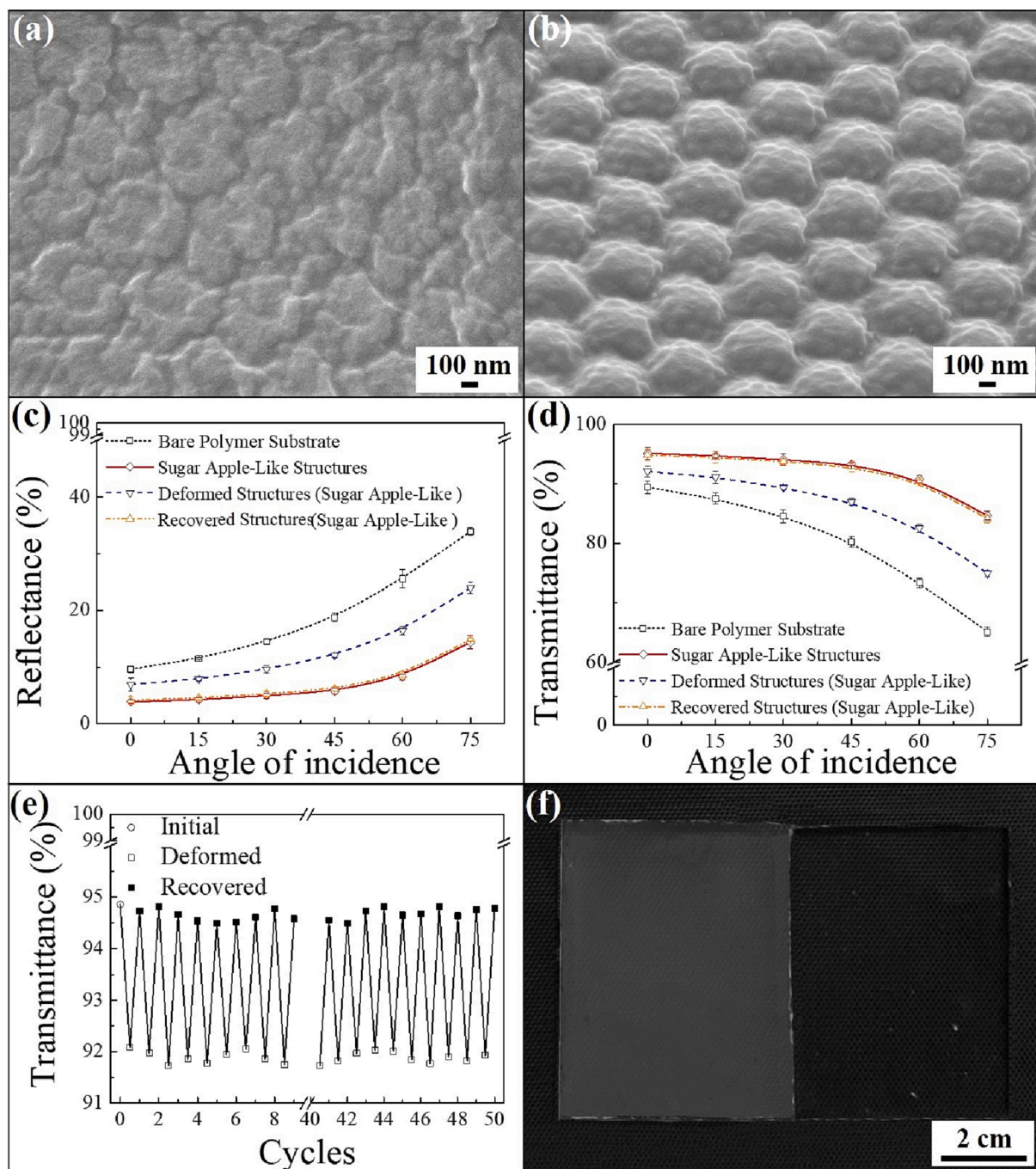
Fig. 8. SEM images of (a) temporarily deformed and (b) recovered sugar apple-like structure arrays. (c) Average reflectances and (d) average transmittances in the visible spectral range collected from a bare polymer substrate (black curve) and polymer substrates covered with hexagonally arranged sugar apple-like structure arrays (red curve), temporarily deformed sugar apple-like structure arrays (blue curve), and recovered sugar apple-like structure arrays (orange curve) at varied incident angles. (e) Switchable antireflective characteristics of the sugar apple-like structure arrays triggered by ethanol drying. (f) Photographic images of a polymer substrate covered with temporarily deformed sugar apple-like structure arrays (the left half) and recovered sugar apple-like structure arrays (the right half) after 50 deforming/recovering cycles. The image is taken under natural illumination. (For interpretation of the references to colour in this figure legend, the reader is referred to the web version of this article.)

deformed hieratical structure array can be preserved for at least 6 months. Interestingly, their original configurations are recovered as the deformed structure array-covered specimen is rinsed with absolute ethanol to relax and swell the copolymer network, followed by drying out of ethanol (Fig. 8 (b)). The resulting copolymer expansion eventually leads to the recovery of temporarily deformed structures. It is worthy to note that the low surface tension of ethanol results in a weak evaporation-stimulated capillary force, which is not enough to surpass

the Young's modulus of the copolymer. Without a doubt, optical properties of the hierarchical structure array-covered specimen are associated with the structural transition. As shown in Fig. 8 (c) and (d), the squashed sugar apple-like structures generate a steep refractive index transition, giving rise to increased reflectances and decreased transmittances at various incidence angles (blue dashed curve). In contrast, the omnidirectional antireflection performance is reinstated on a recovered structure array-covered specimen (orange dash-dotted curve).
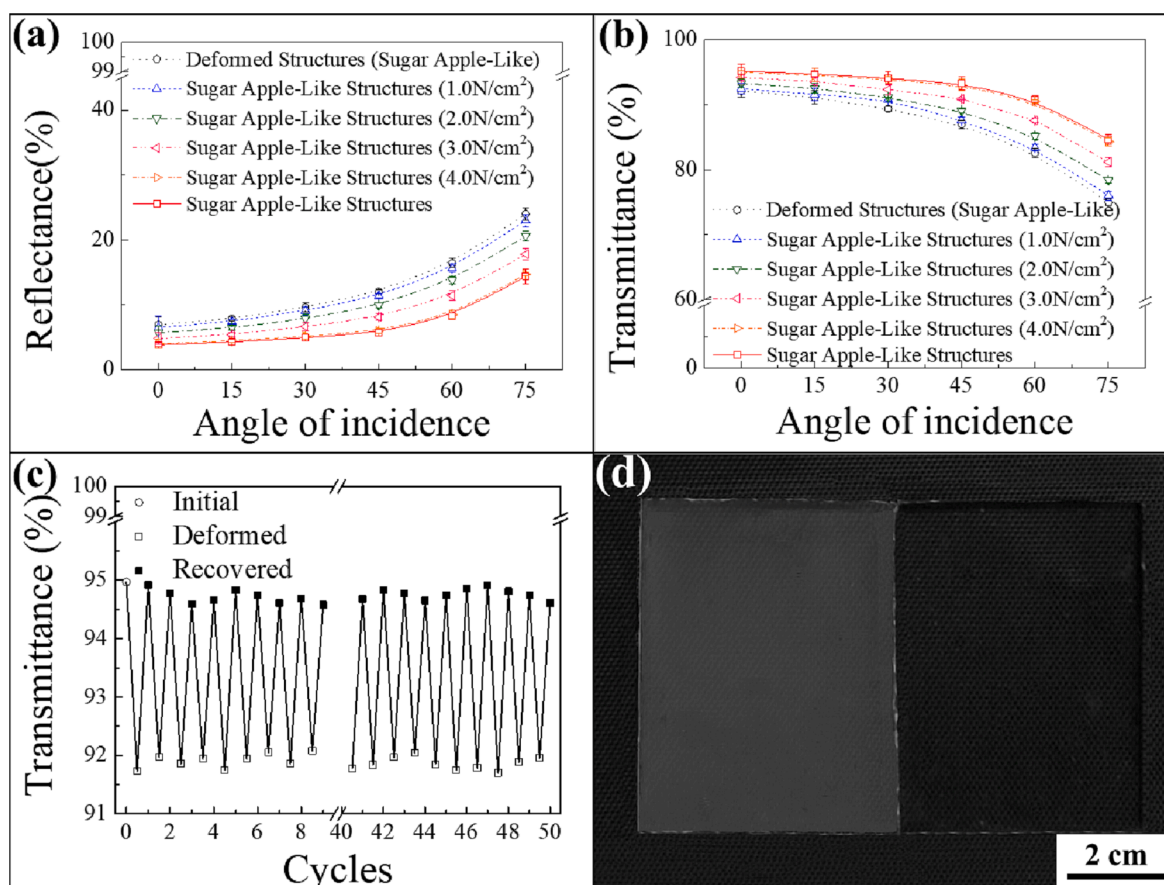
Fig. 9. (a) Average reflectances and (b) average transmittances in the visible spectral range collected from a bare polymer substrate (black curve) and polymer substrates covered with temporarily deformed sugar apple-like structure arrays after applying varied contact pressures of 1.0 N/cm^2 (blue curve), 2.0 N/cm^2 (green curve), 3.0 N/cm^2 (pink curve), and 4.0 N/cm^2 (orange curve) at varied incident angles. (c) Switchable antireflective characteristics of the sugar apple-like structure arrays triggered by applying contact pressures. (d) Photographic images of a polymer substrate covered with temporarily deformed sugar apple-like structure arrays (the left half) and recovered sugar apple-like structure arrays (the right half) after 50 structure deforming/recovering cycles. The image is taken under natural illumination. (For interpretation of the references to colour in this figure legend, the reader is referred to the web version of this article.)

It's average reflectances and transmittances even well match with those of the undeformed structure array-covered specimen (red solid curve), indicating that the broadband omnidirectional antireflective characteristics can be fully recovered. The findings further reveal that a reversible structural transition of hierarchical structures, accompanied by switchable antireflective characteristics, can be triggered by applying demanded solvent drying processes. More importantly, the capillary force-stimulated antireflection-switching ability is highly repeatable for at least 50 structure deforming/recovering cycles (Fig. 8 (e)). In comparison with the pale white appearance of the deformed structure array-covered specimen (left half), the recovered structure array-covered specimen (right half) displays a high optical transparency under natural illumination (Fig. 8 (f)).

In addition to capillary forces, the structural transition can be triggered by external contact pressures. To gain a better comprehension, demanded standard calibration weights are placed on the deformed sugar apple-like structure array-covered specimen, where a glass coverslip is sandwiched in between to ensure that varied contact pressures of 1.0 N/cm^2, 2.0 N/cm^2, 3.0 N/cm^2, and 4.0 N/cm^2 are exerted onto the structures evenly. Once the weights are lifted up, the attractive van der Waals forces generated between the coverslip and the specimen actuate the shape memory recovery instantaneously. Apparently, the application of a higher contact pressure results in a further recovery of sugar apple-like structures (Fig. S7) and an improved omnidirectional antireflection performance (Fig. 9 (a) and (b)). It is worth mentioning that the sugar apple-like structure array and its corresponding

antireflective characteristics are fully restored as a contact pressure of 4.0 N/cm^2 is imposed. The dominancy of contact pressure over the polymer entropy elasticity drives the water evaporation-induced deformed structures to recover their original conformations [48–50]. In other words, the external energy is employed to overcome the shape memory activation barrier, and hence to trigger the shape recovery. As evidenced previously, the restored antireflection performance is impaired by introducing water evaporation-induced capillary forces, and then once again recover right after applying demanded contact pressures (Fig. 9 (c) and (d)). The results further disclose that varying degrees of antireflection capabilities can be reversibly switched by exerting appropriate contact pressures onto the shape-memory artificial brochosomes.

To ensure an environmentally durable operating condition, the capability to withstand superficial mechanical forces is of great importance for antireflection coatings. Herein, a constant-load scratch resistance examination in accordance with the ASTM D3363 method is performed using standard pencils with hardness grades of 1H to 9H for evaluating the mechanical robustness of as-engineered silica hollow sphere-embedded sugar apple-like structure array-covered specimen [51,52]. The selected pencil is polished by a sandpaper, and then placed on the specimen with a 45° angle under a load of 10 N. In the experiment, the coating hardness is considered the highest pencil hardness grade that insufficient to damage the specimen surface after 1000 rubbing cycles. As exhibited in Fig. 10 (a) and (b), increased reflectances and diminished transmittances at varied incident angles are identified as
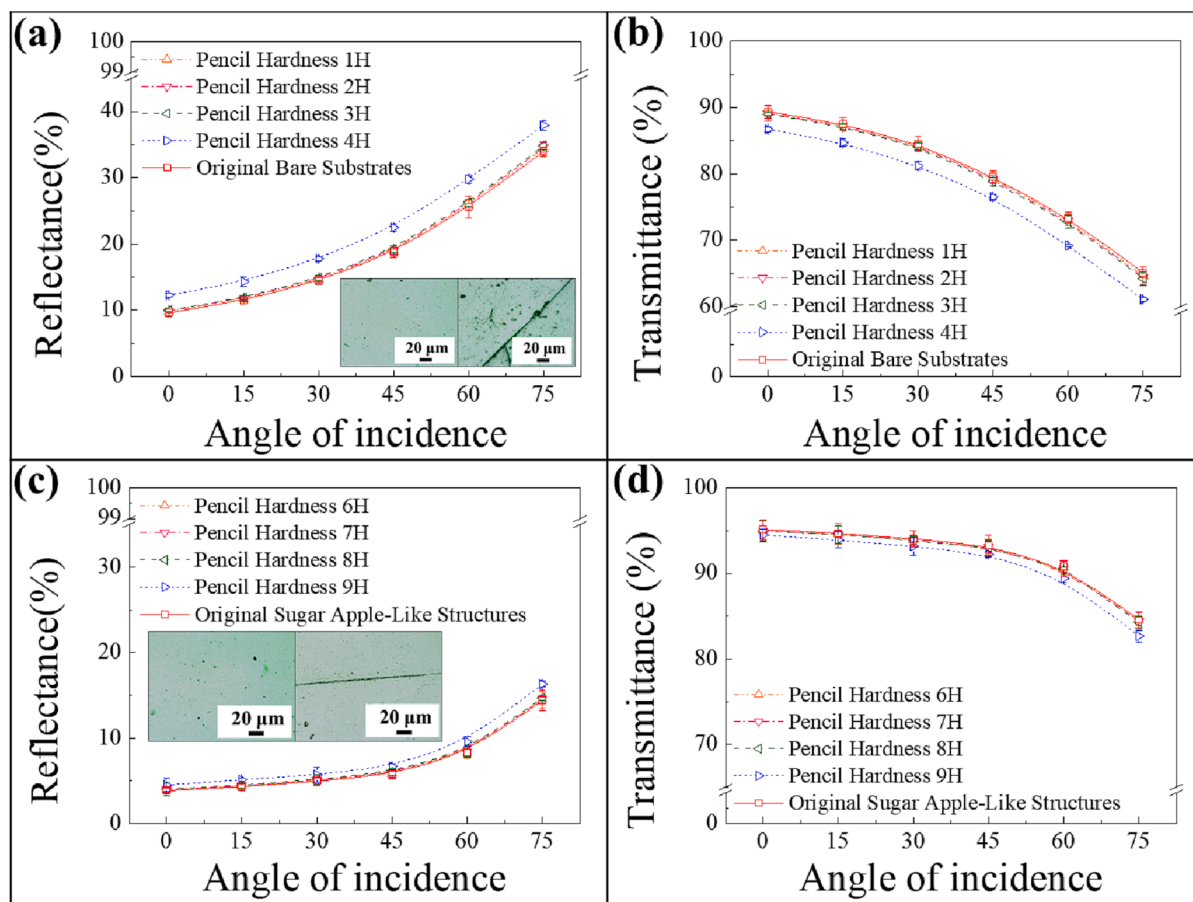
Fig. 10. (a) Average reflectances and (b) average transmittances in the visible spectral range collected from bare polymer substrates before and after pencil scratching tests at varied incident angles. The inserts showing surface morphologies of the bare polymer substrates before (the left one) and after (the right one) scratching with a 4H pencil. (c) Average reflectances and (d) average transmittances in the visible spectral range collected from sugar apple-like structure-covered polymer substrates before and after pencil scratching tests at varied incident angles. The inserts showing surface morphologies of the structure-covered polymer substrates before (the left one) and after (the right one) scratching with a 9H pencil.

a featureless specimen is scratching with a 4H pencil. The impaired antireflective properties are attributed to distinct traces of scratches on the specimen surface (inserts of Fig. 10 (a)). By contrast, the antireflective properties of a sugar apple-like structure array-covered specimen are well-maintained even after an 8H pencil hardness examination (Fig. 10 (c) and (d)), which is competitive with commercial antireflection coatings [53]. Apparently, the incorporation of silica hollow spheres as reinforcing fillers significantly enhances the mechanical robustness.

4. Conclusions

Bioinspired by small yellow leafhoppers, a non-photolithography-based methodology is developed to self-assemble stimuli-responsive silica hollow sphere-embedded hierarchical structures using an ambient-temperature shape memory polymer. The resulting hexagonally arranged sugar apple-like structure array establishes a moderate refractive index transition, and therefore brings about broadband omnidirectionally antireflective characteristics. Benefiting from its shape memory behaviors, varying degrees of antireflection performances can be reversibly switched through applying either demanded solvent evaporation-induced capillary forces or appropriate contact pressures. Importantly, the introduction of silica spheres greatly enhances the capability of the antireflection coating to withstand superficial mechanical forces and ensure an environmentally durable operating condition, which provides a facile strategy for developing a variety of smart optical applications.

CRediT authorship contribution statement

Kuan-Ting Chiang: Methodology, Writing – original draft. **Shin-Hua Lin:** Writing – original draft. **Yu-Zhe Ye:** Writing – original draft. **Bo-Han Zeng:** Writing – original draft. **Ya-Lien Cheng:** Writing – original draft. **Rong-Ho Lee:** Writing – original draft. **Kun-Yi Andrew Lin:** Conceptualization, Writing – original draft. **Hongta Yang:** Conceptualization, Writing – review & editing, Supervision, Project administration, Funding acquisition.

Declaration of Competing Interest

The authors declare that they have no known competing financial interests or personal relationships that could have appeared to influence the work reported in this paper.

Data availability

Data will be made available on request.

Acknowledgments

MOST 110-2221-E-005-050-MY2), and the Instrument Center of National Chung Hsing University for the technical supports with scanning electron microscope.

Appendix A. Supplementary data

Supplementary data to this article can be found online at https://doi.org/10.1016/j.jcis.2023.06.179.

References

[1] H. Sun, J.X. Liu, C. Zhou, W.H. Yang, H. Liu, X. Zhang, Z.H. Li, B.B. Zhang, W. Q. Jie, Y.D. Xu, Enhanced transmission from visible to terahertz in znte crystals with scalable subwavelength structures, ACS Appl. Mater. Interfaces 13 (14) (2021) 16997–17005.

[2] Z.G. Wang, K. Yu, S.J. Gong, H.B. Mao, R. Huang, Z.Q. Zhu, Cu_3BiS_3/MXenes with excellent solar-thermal conversion for continuous and efficient seawater desalination, ACS Appl. Mater. Interfaces 13 (14) (2021) 16246–16258.

[3] M. La, H.J. Zhou, N. Li, Y.C. Xin, R. Sha, S.H. Bao, P. Jin, Improved performance of Mg-Y alloy thin film switchable mirrors after coating with a superhydrophobic surface, Appl. Surf. Sci. 403 (2017) 23–28.

[4] S.S. Zeng, D.Y. Zhang, W.H. Huang, Z.F. Wang, S.G. Freire, X.Y. Yu, A.T. Smith, E. Y. Huang, H. Nguon, L.Y. Sun, Bio-inspired sensitive and reversible mechanochromisms *via* strain-dependent cracks and folds, Nat. Commun. 7 (2016), 9.

[5] A. Islam, B. Mukherjee, K.K. Pandey, A.K. Keshri, Ultra-fast, chemical-free, mass production of high quality exfoliated graphene, ACS Nano 15 (1) (2021) 1775–1784.

[6] R. Guo, H. Luo, M.Y. Yan, X.F. Zhou, K.C. Zhou, D. Zhang, Significantly enhanced breakdown strength and energy density in sandwich-structured nanocomposites with low-level $BaTiO_3$ nanowires, Nano Energy 79 (2021), 105412.

[7] T.Q. Hou, Z.R. Jia, B.B. Wang, H.B. Li, X.H. Liu, L. Bi, G.L. Wu, MXene-based accordion 2D hybrid structure with $Co_9S_8/C/Ti_3C_2Tx$ as efficient electromagnetic wave absorber, J. Chem. Eng. 414 (2021) 128875.

[8] E. Cho, Y.Y. Kim, D.S. Ham, J.H. Lee, J.S. Park, J. Seo, S.J. Lee, Highly efficient and stable flexible perovskite solar cells enabled by using plasma-polymerized-fluorocarbon antireflection layer, Nano Energy 82 (2021), 11.

[9] A.Q. Xie, J.Z. Guo, L.L. Zhu, S. Chen, Carbon dots promoted photonic crystal for optical information storage and sensing, J. Chem. Eng. 415 (2021), 10.

[10] N. Chen, Y.M. Lee, Anion exchange polyelectrolytes for membranes and ionomers, Prog. Polym. Sci. 113 (2021), 35.

[11] J.J. Wang, X.X. Wang, M.S. AlQahtani, S.D. Knecht, S.G. Bilen, W. Chu, C.S. Song, Synergetic effect of non-thermal plasma and supported cobalt catalyst in plasma-enhanced CO_2 hydrogenation, J. Chem. Eng. 451 (2023), 11.

[12] Y.C. Lin, H.X. Zhang, Y. Zou, K.Y. Lu, L.H.Z. Li, Y. Wu, J.J. Cheng, Y.X. Zhang, H. Chen, Q. Yu, Superhydrophobic photothermal coatings based on candle soot for prevention of biofilm formation, J. Mater. Sci. Technol. 132 (2023) 18–26.

[13] J.H. Li, Y.J. Chen, S.N. He, Y.X. Yang, Y.Z. Wang, L. Guo, High performance $Na_3V_2(PO_4)_3$ with nitrogen-chlorine co-doped carbon matrix in-situ synthesized in chitosan quaternary ammonium hydrogel for sodium ion batteries, J. Chem. Eng. 452 (2023), 14.

[14] C.J. Lai, H.P. Tsai, J.Y. Chen, M.X. Wu, Y.J. Chen, K.Y. Lin, H.T. Yang, Single-step fabrication of longtail glasswing butterfly-inspired omnidirectional antireflective structures, Nanomater. 12 (11) (2022), 9.

[15] C.Y. Chien, Y.H. Chen, R.Y. Chen, H.T. Yang, Dragonfly-wing-inspired inclined irregular conical structures for broadband omnidirectional antireflection coatings, ACS Appl. Nano Mater. 3 (1) (2020) 789–796.

[16] P. Stusek, K. Hamdorf, Properties of pupil mechanisms in owl-fly Ascalaphus macaronius (Neuroptera), J. Comp. Physiol. A-Sens. Neural Behav. Physiol. 184 (1) (1999) 99–106.

[17] V. Narasimhan, R.H. Siddique, J.O. Lee, S. Kumar, B. Ndjamen, J. Du, N. Hong, D. Sretavan, H. Choo, Multifunctional biophotonic nanostructures inspired by the longtail glasswing butterfly for medical devices, Nat. Nanotechnol. 13 (6) (2018) 512–519.

[18] H.Y. Tseng, Y.H. Chen, R.Y. Chen, H.T. Yang, Reversibly erasable broadband omnidirectional antireflection coatings inspired by inclined conical structures on blue-tailed forest hawk dragonfly wings, ACS Appl. Mater. Interfaces 12 (9) (2020) 10883–10892.

[19] C. Cho, J. Oh, B. Lee, B. Kim, Combined effects of pyramid-like structures and antireflection coating on si solar cell efficiency, J. Nanosci. Nanotechnol. 15 (10) (2015) 7624–7631.

[20] R.Y. Chen, C.J. Lai, Y.J. Chen, M.X. Wu, H.T. Yang, Omnidirectional / Unidirectional antireflection-switchable structures inspired by dragonfly wings, J. Colloid Interface Sci. 610 (2022) 246–257.

[21] J.S. Choi, J.H. An, J.K. Lee, J.Y. Lee, S.M. Kang, Optimization of shapes and sizes of moth-eye-inspired structures for the enhancement of their antireflective properties, Polymers 12 (2) (2020), 9.

[22] Z. Wang, H.L. Ding, D.L. Liu, C.H. Xu, B. Li, S.C. Niu, J. Li, L.P. Liu, J. Zhao, J. Q. Zhang, Z.Z. Mu, Z.W. Han, L.Q. Ren, Large-scale bio-inspired flexible antireflective film with scale-insensitivity arrays, ACS Appl. Mater. Interfaces 13 (19) (2021) 23103–23112.

[23] M. Sepulveda, K. Kamnev, Z. Pytlicek, J. Prasek, A. Mozalev, Superhydrophobic-oleophobic visible-transparent antireflective nanostructured anodic HfO_2

[24] multifunctional coatings for potential solar panel applications, ACS Appl. Nano Mater. 4 (2) (2021) 1754–1765.

[24] A. Papadopoulos, E. Skoulas, A. Mimidis, G. Perrakis, G. Kenanakis, G.D. Tsibidis, E. Stratakis, Biomimetic omnidirectional antireflective glass *via* direct ultrafast laser nanostructuring, Adv. Mater. 31 (32) (2019), 8.

[25] X.Z. Ye, L.M. Qi, Two-dimensionally patterned nanostructures based on monolayer colloidal crystals: Controllable fabrication, assembly, and applications, Nano Today 6 (6) (2011) 608–631.

[26] J.D. Williams, W.J. Wang, Study on the postbaking process and the effects on UV lithography of high aspect ratio SU-8 microstructures, J. Microlithogr. Microfabr. Microsyst. 3 (4) (2004) 563–568.

[27] C.G. Nunez, W.T. Navaraj, F.Y. Liu, D. Shakthivel, R. Dahiya, Large-area self-assembly of silica microspheres/nanospheres by temperature-assisted dip-coating, ACS Appl. Mater. Interfaces 10 (3) (2018) 3058–3068.

[28] G.R. Burks, L.H. Yao, F.C. Kalutantirige, K.J. Gray, E. Bello, S. Rajagopalan, S. B. Bialik, J.E. Barrick, M. Alleyne, Q. Chen, C.M. Schroeder, Electron tomography and machine learning for understanding the highly ordered structure of leafhopper brochosomes, Biomacromolecules 24 (1) (2023) 190–200.

[29] Z. Li, Y.Y. Li, A.Z. Xue, V. Dang, V.R. Holmes, J.S. Johnston, J.E. Barrick, N. A. Moran, The genomic basis of evolutionary novelties in a leafhopper, Mol. Biol. Evol. 39 (9) (2022), 13.

[30] R. Rakitov, S.N. Gorb, Brochosomal coats turn leafhopper (Insecta, Hemiptera, Cicadellidae) integument to superhydrophobic state, Proc. R. Soc. B-Biol. Sci. 280 (1752) (2013), 9.

[31] R. Sukamanchi, D. Mathew, S. Kumar, Durable superhydrophobic particles mimicking leafhopper surface: superolephilicity and very low surface energy, ACS Sustainable Chem. Eng. 5 (2017) 252–260.

[32] R. Pakitov, A.A. Moysa, A.T. Kopylov, S.A. Moshkovskii, R.S. Peters, K. Meusemann, B. Misof, C.H. Dietrich, K.P. Johnson, L. Podsiadlowski, K.K. O. Walden, Brochosomins and other novel proteins from brochosomes of leafhoppers (Insecta, Hemiptera, Cicadellidae), Insect Biochem. Mol. Biol. 94 (2018) 10–17.

[33] S.K. Yang, N. Sun, B.B. Stogin, J. Wang, Y. Huang, T.S. Wong, Ultra-antireflective synthetic brochosomes, Nat. Commun. 8 (2017), 8.

[34] Z.G. Li, J.J. Lin, Z.Q. Liu, S.S. Feng, Y.P. Liu, C.F. Wang, Y. Liu, S.K. Yang, Durable broadband and omnidirectional ultra-antireflective surfaces, ACS Appl. Mater. Interfaces 10 (46) (2018) 40180–40188.

[35] R.C.P. Verpaalen, T. Engels, A. Schenning, M.G. Debije, Stimuli-responsive shape changing commodity polymer composites and bilayers, ACS Appl. Mater. Interfaces 12 (35) (2020) 38829–38844.

[36] S. Banisadr, A. Oyefusi, J. Chen, A versatile strategy for transparent stimuli-responsive interference coloration, ACS Appl. Mater. Interfaces 11 (7) (2019) 7415–7422.

[37] N. Zhao, Z. Wang, C. Cai, H. Shen, F.Y. Liang, D. Wang, C.Y. Wang, T. Zhu, J. Guo, Y.X. Wang, X.F. Liu, C.T. Duan, H. Wang, Y.Z. Mao, X. Jia, H.X. Dong, X.L. Zhang, J. Xu, Bioinspired materials: from low to high dimensional structure, Adv. Mater. 26 (41) (2014) 6994–7017.

[38] Y. Fang, S.Y. Leo, Y.L. Ni, J.Y. Wang, B.C. Wang, L. Yu, Z. Dong, Y.Q. Dai, V. Basile, C. Taylor, P. Jiang, Reconfigurable photonic crystals enabled by multistimuli-responsive shape memory polymers possessing room temperature shape processability, ACS Appl. Mater. Interfaces 9 (6) (2017) 5457–5467.

[39] D. Meng, Q.L. Zhao, X.Y. Cheng, J.H. Ma, L.Y. Kong, X.H. He, J.W. Li, Water-induced shape memory cellulose nanofiber-based nanocomposite membrane containing lignin with quick water response and excellent wet mechanical property, Eur. Polym. J. 171 (2022), 10.

[40] Y. Li, H.M. Chen, D. Liu, W.X. Wang, Y. Liu, S.B. Zhou, pH-Responsive shape memory poly(ethylene glycol)-poly(epsilon-caprolactone)-based polyurethane/cellulose nanocrystals nanocomposite, ACS Appl. Mater. Interfaces 7 (23) (2015) 12988–12999.

[41] S.Y. Leo, Y.L. Ni, C. Xu, Y.F. Zhang, Y.Q. Dai, P.X. Qi, A.T. Xie, V. Basile, C. Taylor, P. Jiang, Programmable macroporous photonic crystals enabled by swelling-induced all-room-temperature shape memory effects, Adv. Funct. Mater. 27 (41) (2017), 11.

[42] W. Stober, A. Fink, E. Bohn, Controlled growth of monodisperse silica spheres in micron size range, J. Colloid Interface Sci. 26 (1) (1968) 62–69.

[43] P. Galanopoulou, N. Gil, D. Gigmes, C. Lefay, Y. Guillaneuf, M. Lages, J. Nicolas, M. Lansalot, F. D`Agosto, One-step synthesis of degradable vinylic polymer-based latexes *via* aqueous radical emulsion polymerization, Angew. Chem. Int. Ed. 61 (15) (2022).

[44] Z.G. Teng, W. Li, Y.X. Tang, A. Elzatahry, G.M. Lu, D.Y. Zhao, Mesoporous organosilica hollow nanoparticles: Synthesis and applications, Adv. Mater. 31 (38) (2019), 1707612.

[45] G.Y. Yoo, N. Nurrosyid, S. Lee, Y. Jeong, I. Yoon, C. Kim, W. Kim, S.Y. Jang, Y. R. Do, Newly developed broadband antireflective nanostructures by coating a low-index MgF_2 film onto a SiO_2 moth-eye nanopattern, ACS Appl. Mater. Interfaces 12 (9) (2020) 10626–10636.

[46] P. Kothary, X. Dou, Y. Fang, Z.X. Gu, S.Y. Leo, P. Jiang, Superhydrophobic hierarchical arrays fabricated by a scalable colloidal lithography approach, J. Colloid Interface Sci. 487 (2017) 484–492.

[47] H.T. Yang, X. Dou, Y. Fang, P. Jiang, Self-assembled biomimetic superhydrophobic hierarchical arrays, J. Colloid Interface Sci. 405 (2013) 51–57.

[48] Y. Fang, Y.L. Ni, B. Choi, S.Y. Leo, J. Gao, B. Ge, C. Taylor, V. Basile, P. Jiang, Chromogenic photonic crystals enabled by novel vapor-responsive shape-memory polymers, Adv. Mater. 27 (24) (2015) 3696–3704.

[49] Y. Fang, Y.L. Ni, S.Y. Leo, C. Taylor, V. Basile, P. Jiang, Reconfigurable photonic crystals enabled by pressure-responsive shape-memory polymers, Nat. Commun. 6 (2015), 7416.

[50] C.J. Leverant, S.-Y. Leo, M.A. Cordoba, Y. Zhang, N. Charpota, C. Taylor, P. Jiang, Reconfigurable anticounterfeiting coatings enabled by macroporous shape memory polymers, ACS Appl. Polym. Mater. 1 (2019) 36–46.

[51] F.T. Chi, D.J. Liu, H.Y. Wu, J.H. Lei, Mechanically robust and self-cleaning antireflection coatings from nanoscale binding of hydrophobic silica nanoparticles, Sol. Energy Mater Sol. Cells 200 (2019), 109939.

[52] Y.Q. Li, L. Zhang, C.Z. Li, Highly transparent and scratch resistant polysiloxane coatings containing silica nanoparticles, J. Colloid Interface Sci. 559 (2020) 273–281.

[53] R. Sagar, A. Rao, Nanoscale TiO_2 and Ta_2O_5 as efficient antireflection coatings on commercial monocrystalline silicon solar cell, J. Alloys Compd. 862 (2021), 158464.